

CHAPTER 1

**VELOCITY MAPPING STUDIES
OF MOLECULAR PHOTODISSOCIATION
AND PHOTOIONIZATION DYNAMICS**

David H. Parker

*Dept. of Molecular and Laser Physics, University of Nijmegen
Toernooiveld 1, 6525 ED Nijmegen, The Netherlands*

E-mail: parker@sci.kun.nl

Contents

1. Introduction	4
1.1. REMPI, through a Looking Glass	4
1.2. Newton Spheres	7
1.3. Velocity Mapping in Photodissociation and Photoionization Studies	10
1.3.1. Photodissociation Studies	10
1.3.1.1. Correlation of internal state and velocity distributions	11
1.3.1.2. Directional properties	12
1.3.1.3. Angular distributions — the (μ, ν) correlation, the time-scale of photodissociation, and the spectroscopic signature of excited electronic states	13
1.3.1.4. The (μ, ν, \mathbf{J}) three-vector correlation	15
1.3.1.5. Coherence effects	16
1.3.2. Photoelectron Studies	17
2. Experimental Section	18
2.1. Apparatus	18
2.1.1. Resolution: Factors Affecting Image Quality	20
3. Applications of Velocity Mapping	25
3.1. Decomposition of Absorption Continua: Neutral Product Analysis	25

3.1.1. Decomposition of the A-Band of Halogen Containing Species	27
3.1.2. Decomposition of the Herzberg Continuum of Molecular Oxygen	34
3.2. Predissociation Angular Distributions — State Lifetimes	37
3.3. Super-Excited States	42
4. Conclusions	44
References	44

1. Introduction

1.1. REMPI, through a Looking Glass

Almost any experiment using laser ionization, including many described in this volume, should be using velocity mapping. I hope to convince the reader of this, using several examples of recent velocity mapping studies as illustration. Velocity mapping is essentially a means of extracting all the information possible from a REMPI (resonance-enhanced multiphoton ionization) measurement. REMPI has, over the years, become one of the most-used laboratory methods in molecular spectroscopy and dynamics. Consider Fig. 1, a schematic diagram of REMPI spectroscopy experiments that became common in the 1970s, shortly after the introduction of nitrogen-laser-pumped dye lasers. In typical experiments of this era, a pulsed tunable laser beam was focused into a cell between two electrodes and current, A , in the circuit is measured with a sensitive electrometer. On scanning the dye laser wavelength, peaks observed in the current correspond to electronic states resonant with the energy sum of one or several

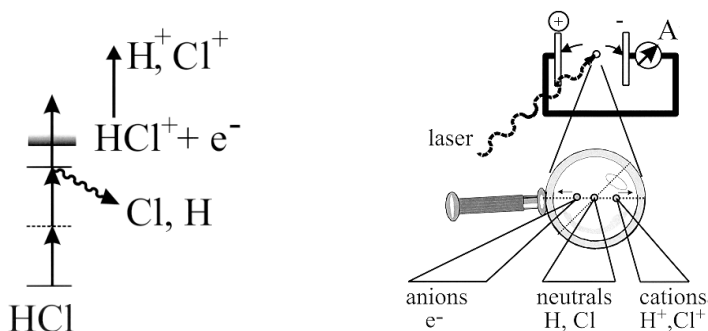


Fig. 1. Schematic diagram of a REMPI experiment for (2+1) ionization and dissociation processes in HCl.

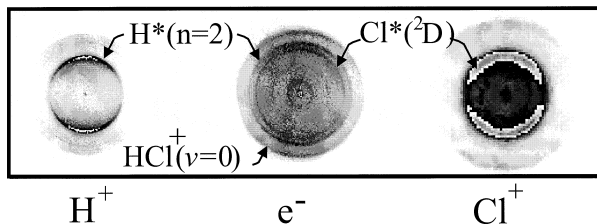


Fig. 2. Velocity maps of the charged species formed in (2 + 1) REMPI of HCl at 234.5 nm. In each image the laser polarization lies along the vertical axis. Darker areas correspond to higher signal levels, except for off-scale white areas in the strongest rings. The Cl^+ image has been magnified by a factor of ~ 8 .

of the laser photons. An excited electronic state at the two-photon level results in an enhancement of parent ion production after absorption of a third photon, a so-called (2 + 1) REMPI process. As indicated in the energy level diagram, after the initial photoabsorption step a molecule such as HCl can fragment or absorb more photons to form ions, which can themselves undergo photofragmentation. Analysis of the parent ion signals and those of the fragments as a function of laser wavelength has led to tremendous progress in the last two decades in the understanding of higher-energy electronically excited states and their dissociation dynamics.¹

There is much more information available from REMPI, however, if one looks in more detail — through a powerful magnifying glass — at the velocity distributions of the different ionic species formed in the ionization process. Imagine that one could look through the electrodes in Fig. 1 at the charged species as they arrive. Under the right conditions beautiful patterns can be seen, a few of which are shown in Fig. 2. Instead of arriving at a single point, the ions deviate from the line connecting the laser focus and electrode because they have gained kinetic energy from the photoabsorption process. For example, in the energy level diagram in Fig. 1 the molecule HCl absorbs two photons and fragments, producing neutral H and Cl atoms which recoil with a kinetic energy determined by the difference in the energy sum of two photons and D_0 , the bond energy. From the two-photon state another photon could ionize the molecule, creating photoelectrons which recoil with energy determined by the difference in the energy sum of three photons and the molecular ionization potential. These electrons fly towards the positive electrode. The HCl^+ molecular ions formed, which receive negligible recoil from the photoionization step, fly towards the negative electrode. During the laser pulse a fourth photon can dissociate the

HCl^+ , creating H and Cl^+ (or H^+ and Cl) fragments with kinetic energies determined by the photon energy and D_0^+ , the molecular ion bond energy. These cationic fragments fly towards the negative electrode. It is also possible that a fourth photon could ionize an electronically excited neutral H^* or Cl^* atoms, creating another source of electrons and ions. Furthermore, ground state neutral fragments, such as those created at the two-photon level could also be converted into ions in another REMPI process with a separate pulsed laser system. Since ionization hardly changes the kinetic energy of the heavy cation formed, the pattern seen at the electrode will be that of the ground state neutral species.

Velocity mapping is the powerful magnifying glass that allows us to see the spatial patterns of the different ionic fragments formed in REMPI. As can be imagined, special effort is needed to obtain such sharp images as shown in Fig. 2. It turns out that the most important trick is devising a method of measuring only the velocity of the species in a manner that is independent of their position of origin. These velocity patterns (images) are two-dimensional (2-D) projections of 3-D Newton spheres, and as described in the next section, all of the information on the photophysics is contained in the Newton sphere. Going back to the example in Figs. 1 and 2 for HCl, the REMPI process of focusing 234.5 nm pulsed laser radiation forms H^+ , Cl^+ , HCl^+ , and photoelectrons. Using the apparatus described in the experimental section, the velocity patterns of each ion can be measured separately, and when the information from the images is combined, a very detailed view of the REMPI photodissociation/photoionization processes taking place can be extracted. A few of the related signals in the different images are identified in Fig. 2 for the most active channels. For example, absorption of three 234.5 nm photons results in the formation of super-excited HCl^{**} which dissociates, producing electronically excited Cl and H atoms that recoil with a fixed kinetic energy.

Photoelectrons formed from the subsequent photoionization of these electronically excited atoms are seen in the photoelectron image with a characteristic angle-velocity distribution determined by the atomic photoionization process. The partner Cl^+ atoms, labeled in the Cl^+ image, show the angle-velocity distribution of the HCl^{**} dissociation process, since photoionization hardly affects the initial neutral atom velocity. Similar information is available from the strongest signal in the H^+ image, which arises from photoionization of $\text{H}(n=2)$ atoms. The numerous other channels seen in the photoelectron image are due to production of HCl^+ vibrational levels.

In this case, the HCl^+ partner receives only a minuscule recoil from the photoionization; thus the velocity map shows one point which corresponds to zero velocity. Products from photodissociation of these different HCl^+ vibrational levels are seen in the H^+ and Cl^+ images. In one image, for example, angular distributions from the photodissociation of at least 10 different ro-vibrationally state-selected HCl^+ ions are determined.

Note in Fig. 2 that images of similar quality are obtainable for very different ion charge/mass ratios, from electrons to chlorine ions. Energy resolution is also quite reasonable — in most cases channels corresponding to ion vibrational levels and often their spin-orbit splitting are well separated. In the following experimental section the resolution and other aspects of velocity mapping will be described, followed by an applications section where more information on superexcited states, which govern the final product characteristics, will be given in more detail.

Velocity mapping is a new variant of the ion imaging technique² that was introduced in 1987 by Chandler and Houston.³ Because the image quality is so much improved over conventional ion imaging a new name for the technique, velocity mapping, has been suggested.⁴ At the time of preparing this article there have been only a handful of articles published using the method. I have thus taken the easiest path and describe mainly work from Nijmegen with the emphasis on the potential of the technique, instead of an in-depth review of one research field. The applications found so far are broad and exciting enough in my mind to warrant this rather limited approach, and I hope the main players in the ion imaging field, which include David Chandler (Livermore), Paul Houston (Cornell), Hanna Reisler (Los Angeles), Arthur Suits (Berkeley), Theofanis Kitsopoulos (Heraklion), Toshinoro Suzuki (Okazaki), and Mike Ashfold (Bristol), and others, will forgive me!

1.2. *Newton Spheres*

Most processes in molecular dynamics⁵ are usually simple two-body events that end with the particles departing from each other with a fixed amount of kinetic energy. This includes chemical reactions $\text{A} + \text{BC} \rightarrow \text{ABC}^* \rightarrow \text{AB} + \text{C}$; inelastic scattering $\text{AB}(v, J) + \text{C} \rightarrow \text{ABC}^+ \rightarrow \text{AB}(v', J') + \text{C}$; photoionization $\text{AB} + h\nu \rightarrow \text{AB}^* \rightarrow \text{AB}^+ + \text{e}^-$; and photodissociation $\text{AB} + h\nu \rightarrow \text{AB}^* \rightarrow \text{A} + \text{B}$, where $\text{AB}(\text{C})^*$ is a transient collision or photoexcited complex. Consider a general process: $\text{AB}^* \rightarrow \text{A} + \text{B} + \text{KER}$ where KER (Kinetic Energy Release) is the excess energy left over after partitioning of

internal energy in the A and B products. Conservation of momentum and energy results in the kinetic energy partitioning $KE_A = (M_B/M_{AB})^* KER$ and $KE_B = (M_A/M_{AB})^* KER$. In the following text, the factor (M_A/M_{AB}) or (M_B/M_{AB}) will be called the mass partitioning factor. For photoionization, $M_{e^-} \ll M_{M^+}$, thus the photoelectron receives essentially all of the KER, while for photodissociation of a homonuclear diatomic such as O_2 , the KER is equally shared between the two product O atoms. In reactive or inelastic scattering, the laboratory velocity of the reactants must also be included in predicting the observed final product velocity. This chapter will focus primarily on photodissociation and photoionization, where the measured product velocity is usually the same in the laboratory as in the center-of-mass frame. Each photodissociation or photoionization event yields two partner fragments with equal momenta flying in opposite directions in the center-of-mass frame. Under the same initial conditions, a second event will produce a pair of fragments flying in another direction but with the same speed — lying thus on the same pair of three-dimensional spheres as the first. These are the so-called Newton spheres for the process. By repeating the process thousands of times, a continuous view of the Newton sphere emerges with a fixed radius and a characteristic intensity pattern on its surface.

A simple 3-D Newton sphere is drawn in Fig. 3 along with the standard polar coordinates r (not shown), θ , and ϕ , where θ is defined with respect to the z -axis (vertical axis in the figure), ϕ is the azimuth angle, and r , the sphere radius. There is a fixed time period between formation and projection of the Newton sphere, thus the sphere radius is directly proportional to velocity. Most of the surface intensity of this sphere is at the poles, representative of a typical $\cos^2 \theta$ distribution. Projection of the sphere onto a 2-D surface will then form a filled circle with most of the intensity at the top and bottom outside edges of the circle. The examples of velocity maps shown in Fig. 2 for REMPI of HCl are simply, and beautifully, the 2-D projections of the collection of all Newton spheres for the numerous photodissociation and photoionization processes that create the same charged species.

The distribution of particles on the surface of a Newton sphere is often anisotropic, as in Fig. 3, especially when linearly polarized light is used as the photoexcitation source. This arises because the excitation process is governed by the transition dipole, which has a directionality in the molecular frame. Molecules in a gas sample that happen to lie with their transition

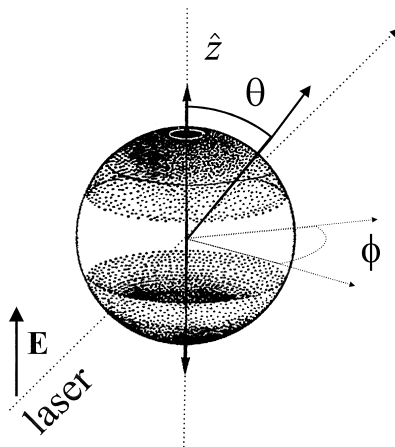


Fig. 3. A 3-D Newton sphere with a $\cos^2 \theta$ angular distribution. Radial co-ordinates, ϕ are shown along with \hat{z} , the usual direction of the laser polarization in the laboratory frame.

dipoles parallel to the polarization vector of the light source are preferentially excited. For photoionization, this defines a laboratory-frame axis for describing the ejected electron waves, which are coherent sums of the possible $s, p, d, f \dots$ wavefunctions. For photodissociation, the directionality of the ejected fragments with respect to the polarization axis depends often on the time-scale of the process. If photodissociation is fast compared to molecular rotation, as in the photodissociation of HCl^+ with ultraviolet light, the line connecting the two fragments (the bond axis, which defines the fragment velocity vector \mathbf{v}) will have a directional correlation, i.e. an alignment, with respect to the electric field vector of the light source. This is apparent in the HCl^+ image in Fig. 2 as a proclivity for fragments at the poles of the sphere, i.e., along the vertical axis, which also is the \mathbf{E} field direction in the figure. Even if dissociation is slow so that the alignment of the dissociation axis is isotropic in the lab frame, the internal angular momentum, J , in each fragment, a measurable quantity, can still be aligned (another so-called vector correlation) along the dissociation axis. These angular momentum and velocity alignments yield direct and highly insightful information on the nature and dynamics of the dissociative electronic states of the target molecule.

Characterization of the Newton spheres of the fragment, including possible vector correlations, requires careful repetition of the experiment under

identical initial conditions. As can be imagined, the most difficult initial condition is the point of origin of the sphere, which must be, of course, a finite volume. One may think that the dimension of the origin must always be directly reflected as a spread in the radius of the ion sphere. With a properly designed apparatus this is not necessarily true. When the particle to be detected is an ion, an electrostatic lens can be used to guide the particle towards the detector. Under the right conditions⁴ the lens maps all particles with the same velocity, $v(v = [2 \times \text{KE}/m]^{1/2})$, to the same point on the two-dimensional detector, irrespective of their positions of origin. Such an electrostatic lens, in our case an immersion lens, once set at the proper voltages, works independently of the particle charge/mass ratio, thus for fast electrons as well as for slow, heavy cations. If the experiment is designed so that the initial AB* velocity is negligible compared to the product velocity, the Newton sphere projected in the laboratory frame (perpendicular to z -axis in Fig. 3), and onto a two-dimensional (2-D) position sensitive detector (PSD), will reflect only the desired center-of-mass information. This can be retrieved from the 2-D image by a mathematical procedure called an inverse Abel transformation.²

1.3. Velocity Mapping in Photodissociation and Photoionization Studies

Under the right conditions, which are outlined in the experimental section, it is possible to reveal Newton spheres in a REMPI experiment. In this section, the motivations for doing so will be outlined. What sort of information on photodissociation⁶ and photoionization⁷ can be gleaned from velocity mapping?

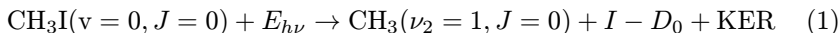
1.3.1. Photodissociation Studies

To begin with, REMPI produces charged species, thus, using mass spectrometry, the most fundamental question in any bimolecular event can be answered, i.e. the chemical nature of the products. One of the next most important questions is the internal energy distribution of the products. REMPI is a state-selective process, thus, in principle this information can also be obtained, but a large number of velocity maps must be measured, one for each possible quantum state produced. Here, it is important to realize that in photodissociation processes the information is doubled, in

that the velocity distribution of one product is correlated with the state distribution of the partner product.

1.3.1.1. Correlation of internal state and velocity distributions

Consider the process:



where $E_{h\nu}$ is the photon energy, $(\nu_2 = 1, J = 0)$ means the methyl radical is in the lowest rotational state of the first quantum of the ν_2 normal mode, D_0 is the C-I bond energy, and KER is the total kinetic energy release into the CH_3 and I fragments. In Eq. (1) we focus on the formation of the lowest rotational state ($J = 0$) of one particular vibrational state of CH_3 radicals produced in the photodissociation of CH_3I . The iodine atom has two ground states separated by 7606 cm^{-1} , the splitting of the upper and lower $^2P_{1/2}$ - $^2P_{3/2}$ spin-orbit states respectively, hereafter labeled as I^* and I. $\text{CH}_3(\nu_2 = 1, J = 0)$ has 606 cm^{-1} more internal energy than $\text{CH}_3(\nu = 0, J = 0)$. If $\text{CH}_3(\nu_2 = 1, J = 0)$ is state-selectively detected, its kinetic energy release (the measured kinetic energy divided by the mass partition factor) can only be $E_{h\nu} - D_0 - 606 \text{ cm}^{-1}$, if I atoms are formed; or $E_{h\nu} - D_0 - 8212 \text{ cm}^{-1}$ if I^* atoms are formed. There can only be two peaks in the $\text{CH}_3(\nu_2 = 1, J = 0)$ velocity map, and the peak height is proportional to the relative population of I or I^* formed in conjunction with $\text{CH}_3(\nu_2 = 1, J = 0)$. Thus, the velocity measurement of one state-selectively detected fragment reveals the correlated state distribution of the other, in this case, two possible fragments. Of course, the situation becomes quite complex when each partner has a large number of possible final states, which is why in most velocity mapping studies so far, at least one of the partners is an atom with a simple ground electronic state structure.

When the I atom is measured with velocity mapping, the population of all CH_3 internal states formed in the $\text{CH}_3 + \text{I}$ channel is revealed in the velocity distribution. While this is quite efficient, the presence of so many possible internal states (CH_3 has four different normal vibrational modes, not to mention the large number of possible J states) often yields an overlapped continuous distribution with limited state-specific information. In CH_3I dissociation, the number of possible CH_3 products states is restricted,⁸ thus, useful information can be obtained from both the CH_3 and I velocity map images.

1.3.1.2. Directional properties

Two more vital pieces of information besides the KER distribution are contained in a velocity map image of a photofragment. One is the intensity pattern on the surface of the Newton sphere, and the other, the variation of this surface distribution with M , the magnetic quantum number. An infinite series of spherical Legendre polynomials can be used to describe an arbitrary surface intensity pattern. Fortunately, because of cylindrical symmetry, the series contains only the even-numbered polynomials and can usually be terminated at P_2 , the second Legendre polynomial for most photodissociation processes. As mentioned previously, molecules whose transition dipoles lie parallel with the polarization direction of the light field \mathbf{E} are preferentially excited. The absorption cross section, $\sigma(\nu)$, a scalar property, for absorption of photons of frequency ν , is given by:

$$\sigma(\nu) \propto \nu_{fi} |\langle \Psi_f | \mathbf{E} \cdot \boldsymbol{\mu} | \Psi_i \rangle|^2 \quad (2)$$

where Ψ_f and Ψ_i represent the final and initial states, whose energies differ by $h\nu_{fi}$; \mathbf{E} is a unit vector along the polarization direction of the electric field, and $\boldsymbol{\mu}$ is the electric dipole operator. The $\mathbf{E} \cdot \boldsymbol{\mu}$ term in Eq. (2) introduces directionality in the process. Taking the Born–Oppenheimer approximation for the separation of electronic and nuclear motion, Eq. (2) simplifies to a probability for a normal one-photon excitation proportional to $\cos^2 \theta$, where θ is the angle between \mathbf{E} (usually defined along the z -axis in the lab frame as in Fig. 3), and $\boldsymbol{\mu}$, the transition dipole which is in the molecular body-fixed frame of reference. Three vectors describe the photodissociation process: (i) $\boldsymbol{\mu}$ in the body-fixed frame (and thus also \mathbf{E} in the lab frame at the moment of photoexcitation); (ii) \mathbf{v} , the fragment recoil velocity vector, and (iii) \mathbf{J} , the rotational angular momentum of the fragments. All three of these vectors can be correlated to each other separately in pairs: $(\boldsymbol{\mu}, \mathbf{v})$ which is the fragment angular distribution in the lab frame, (\mathbf{v}, \mathbf{J}) the fragment angular momentum alignment at the moment of dissociation (which does not have to be locked to the lab frame), and $(\boldsymbol{\mu}, \mathbf{J})$ the product rotational alignment in the lab frame. In addition a $(\boldsymbol{\mu}, \mathbf{v}, \mathbf{J})$ three-vector correlation is possible, which is most revealing for the photodissociation dynamics as is described in more detail later in this chapter for Cl_2 .

types of dissociation processes

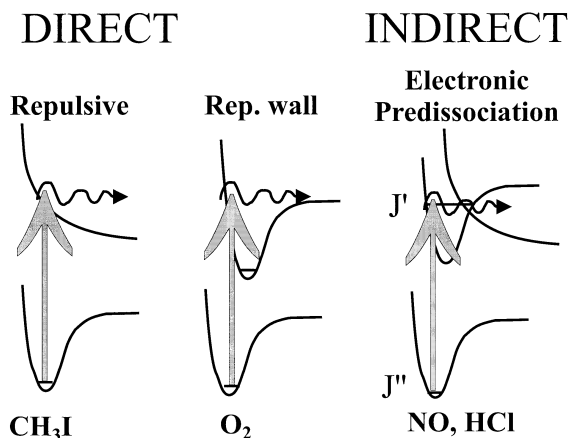


Fig. 4. Direct and indirect photodissociation processes.

1.3.1.3. *Angular distributions — the (μ, \mathbf{v}) correlation, the time-scale of photodissociation, and the spectroscopic signature of excited electronic states*

At this point, it is helpful to describe a photodissociation process as either direct, taking place within one vibrational period of the molecule, or indirect, taking place over at least several vibrational periods. Figure 4 illustrates schematically the different types of direct and indirect processes that will be described in this chapter. Potential energy surfaces (PESs) are shown for three cases, direct photodissociation via a repulsive excited electronic state or the repulsive wall of a bound excited electronic state; and indirect photodissociation due to electronic predissociation. Other types of photodissociation are described in detail by Herzberg⁹ and in a general monograph by Schinke,⁶ or for diatomic molecules in a monograph by Field and LeFevbre-Brion.¹⁰ Examples of direct dissociation will be given later for halogen-containing molecules such as CH₃I, where purely repulsive states are involved, and for molecular oxygen, where the photoexcitation is to electronic states above their bond dissociation energy. In both examples, several overlapping electronic excited states are involved, which, however, complicates the analysis.

An important difference between direct and indirect photodissociation is that in the latter, the bound molecule quantum numbers, particularly the rotational quantum numbers of the lower and upper states, can be spectroscopically selected. For rapid indirect photodissociation, the rotational wavefunction of the ground electronic state can be projected out as the angular distribution of the dissociating fragments.¹¹ By spectroscopic selection of ro-vibrational levels of a particular excited electronic state, it is also possible to choose the dissociation pathway (i.e., which product states are formed) in indirect photodissociation.¹² This will be illustrated for the molecule NO.

For direct photodissociation and rapid indirect photodissociation, the angular distribution of the fragments reveals in many cases the spectroscopic signature of the initial photoexcitation step. This is quite important because for these types of states, normal spectroscopic tools for upper-state symmetry identification are useless since the absorption spectrum shows little or no structure. In fact, a survey of the absorption spectra of simple molecules in the monograph by Okabe¹³ shows that most of the absorption spectra of almost all molecules are broad, unstructured continua. Velocity mapping and related techniques can thus provide an important tool in the future for understanding the absorption spectra of the majority of rapidly dissociating small molecules.

Excitation of a diatomic molecule to a dissociation continuum causes immediate (axial) repulsion of the two atoms with the recoil velocity \mathbf{v} along the molecular bond axis. Here it is assumed that bond breaking occurs much faster than molecular rotation, which is usually a factor of 10-100 slower than molecular vibration. For a diatomic molecule, $\boldsymbol{\mu}$ lies either parallel or perpendicular to the bond axis, thus when a single electronic state is excited the fragments are ejected preferentially either along or perpendicular to the polarization direction of the laser beam. In general, the (state-dependent) fragment angular distribution is described by:

$$I(\theta) = 1/4\pi[1 + \beta P_2(\cos \theta) + \gamma P_4(\cos \theta) + \dots] \quad (3)$$

where P_2 and P_4 represent the second- and fourth-order Legendre polynomials, respectively, β and γ are anisotropy parameters, and θ is now defined as the angle between the velocity recoil vector \mathbf{v} and the z -axis. Note that, due to cylindrical symmetry around z , ϕ does not appear in Eq. (3).

Velocity images are 2-D projections that must be transformed back to the 3-D sphere, and a slice through the 3-D sphere yields the θ angular dependence. With linear absorption to a single upper state, $\gamma = 0$ and β is either $+2$ (pure parallel transition $\Sigma\text{-}\Sigma$, $\Pi\text{-}\Pi$...) or -1 (pure perpendicular transition $\Sigma\text{-}\Pi$...). Usually the symmetry of the ground electronic state of the molecule is known and this information combined with β yields the upper-state symmetry. Incoherent excitation to a mixture of overlapped repulsive electronic states leads to a value of β between the two extremes, $-1 < \beta < +2$. Multiphoton excitation to a single electronic state, or creation of a coherent superposition of electronic states can lead to non-zero values for γ and to the need for more higher-order terms in Eq. (3).

By measuring the fragments' speed and the angular distribution following the photodissociation process, highly detailed information on the lifetime and electronic nature of the excited parent molecule is revealed. For polyatomic molecules, the transition dipole does not necessarily lie either parallel or perpendicular to the dissociation bond axis. In some cases, the angular distributions combined with rotational state population distributions can still give detailed insight into the structure (e.g., linear vs. bent) of the excited state.

1.3.1.4. *The $(\boldsymbol{\mu}, \boldsymbol{v}, \boldsymbol{J})$ three-vector correlation*

A third property of the Newton sphere is the variation of the surface intensity pattern with M , the magnetic quantum number. M is defined in the lab frame as the projection of \boldsymbol{J} , the total angular momentum (usually ignoring nuclear spin I) on the z axis. From the above discussion, it can be seen that a rapid axial dissociation leads to a strong $(\boldsymbol{\mu}, \boldsymbol{v})$ correlation, thus an anisotropic angular distribution. When one of the products is an atom, another important correlation arises from the Wigner–Witmer⁹ rules and introduces a $(\boldsymbol{\mu}, \boldsymbol{J})$ correlation into the process, yielding for certain conditions the three-vector $(\boldsymbol{\mu}, \boldsymbol{v}, \boldsymbol{J})$ correlation. While examination of this three-vector correlation is extremely informative over the photodissociation process, its presence can introduce an extra complication in the interpretation of the velocity map.

According to the Wigner–Witmer rules, the electronic states of a molecule can be constructed from the electronic states of the separated atoms assuming conservation and non-crossing of states of the same

symmetry. For nearly separated atoms, Hund's case (c) is usually appropriate and Ω is the to-be-conserved quantum number. Ω is the projection of \mathbf{J} , the total (electronic plus spin) angular momentum on the molecular body-fixed bond axis. A single diabatic curve connects the photoexcited dissociative molecular excited electronic state to its separated atom limit. If the molecule stays on this curve from molecule to atoms, then the Ω values (thus M quantum numbers) of the atoms are fully specified. For axial recoil the atomic M values are also locked to \mathbf{v} , resulting in the three-vector correlation. Determination of the M value can indicate whether the diabatic curves are followed. If they deviate from the predicted values of the correlation diagram, curve-crossing process induced by terms left out in the Born–Oppenheimer approximation has taken place. This is a signature of processes taking place during the early stages of the molecular dissociation process.

Three-vector correlations pose problems in interpretation of the velocity image because REMPI is itself an M -dependent detection process. If the velocity is measured along a single direction, then, it is always possible to determine the fragment M -state distribution of a dissociation process by measuring the strength of the REMPI signal at several different laser polarization angles.¹⁴ This is not useful in a single laser imaging experiment however, since the laser polarization direction must always lie parallel to the face of the 2-D detector in order to retain proper cylindrical symmetry for the 2-D to 3-D inversion. In a two-laser imaging experiment where a second laser is used to ionize neutral atoms, the second-laser polarization can be rotated to all angles. This is only useful for qualitative analysis of signal at the poles or equator of the Newton sphere, where the averaging over different ϕ components is less important. Most often, the signal is very weak at one of these two extremes, making a judgment on the angle-dependency of the detection difficult. In this case, simulation of the image by a forward convolution is most useful.

1.3.1.5. Coherence effects

Coherent excitation of two electronic states can lead to very interesting interference phenomena that are beginning to be uncovered more routinely in photodissociation experiments. A most interesting recent development here is the discovery by Zare and coworkers¹⁵ of the presence of top-spin and back-spin in the photofragments of ICl. In this molecule a “mixed

transition” arises from the simultaneous and equal excitation of a perpendicular and parallel transition. The electron cloud oscillates at an angle to the bond axis, and as the molecule dissociates, the breaking of cylindrical symmetry becomes top-spin or back-spin in one fragment and the opposite in the other fragment, in order to conserve the overall symmetry. Top-spin and back-spin can be probed with circularly polarized lasers.¹⁵

1.3.2. Photoelectron Studies

Photoionization and photoelectron spectroscopy⁷ have, like photodissociation dynamics, greatly benefited experimentally in the last decades by the advent of high-power tunable laser systems. Many of the most recent advances in this area can be found in other chapters in this book, and in Ref. 7. Velocity mapping works just as well for electrons as for cations, providing the full photoelectron angle-velocity distribution at any chosen laser wavelength. It is more difficult to detect heavier anionic species, such as H^- produced in the ion-pair process $\text{H}_2 + h\nu \rightarrow \text{H}^+ + \text{H}^-$, since the intense UV lasers used efficiently photo-detach the negative ion. The photo-detached electrons produced give rise to a distinctive signal, however, in the photoelectron image. Photoelectron images are more susceptible to background problems, of course, since all ionization processes produce electrons while not all background ionization processes produce the target cationic species. An important advantage to velocity mapping over the more typical photoelectron time-of-flight methods, including the high-resolution magnetic bottle technique,¹⁶ is that v instead of $1/v$ is measured; thus there is no discrimination against the slowest photoelectrons. This will be illustrated later in the chapter.

One area in particular where velocity mapping is useful in photoelectron studies is in the measurement of angular distributions. As outlined by Reid and Leahy in Ref. 7, photoionization can be treated as a special case of photofragmentation using the same general formalism outlined by Zare,¹⁷ which has been simplified to the form of Eq. (3) above for angular distributions. Higher order terms than γ are more often needed to describe photoelectron angular distributions, and when a stable intermediate state is selected in the REMPI process, photoalignment can result, adding an extra factor in the angular distribution. In this chapter, the photoelectron images shown are used mainly to sort out and identify the multiple channels present in a typical REMPI event.

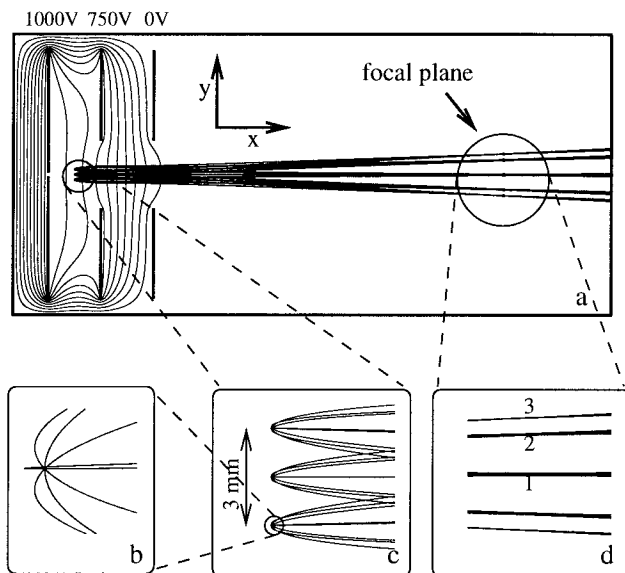


Fig. 5. Apparatus diagram. A cross-section of the electrostatic lens assembly including field lines and ion trajectories is shown.

2. Experimental Section

2.1. Apparatus

Figure 5 shows the key to velocity mapping — an electrostatic immersion lens assembly⁴ — which is simply a set of three flat circular electrodes shown in cross-section. Since the goal of the apparatus is to measure only the recoil velocity of photofragment ions, it is important to minimize the effects of the parent molecule velocity. Entraining the molecule in the supersonic expansion of a pulsed molecular beam, which cools the molecular velocity component transverse to the detection axis down to a few degrees Kelvin or less, does this. The molecular beam passes through a small hole in the first (repeller) electrode where it is intersected at right angles by the photodissociation/REMPI laser(s). An electric field between the repeller and the second (extractor) electrode accelerates the formed ions past the third (ground) electrode, and through a “field-free” time-of-flight (TOF) region and onwards to the 2-D ion detector. The extractor and ground electrodes are thin metal plates with a 15 mm open circle at the middle,